

AutoGNN: End-to-End Hardware-Driven Graph Preprocessing for Enhanced GNN Performance

Seungkwan Kang¹, Seungjun Lee¹, Donghyun Gouk², Miryeong Kwon², Hyunkyu Choi², Junhyeok Jang², Sangwon Lee², Huiwon Choi¹, Jie Zhang³, Wonil Choi⁴, Mahmut Taylan Kandemir⁵, Myoungsoo Jung^{1,2}

*Computer Architecture and Memory Systems Laboratory, KAIST¹, Panmnesia, Inc.²,
Peking University³, Hanyang University⁴, Pennsylvania State University⁵*

Abstract—Graph neural network (GNN) inference faces significant bottlenecks in preprocessing, which often dominate overall inference latency. We introduce AutoGNN, an FPGA-based accelerator designed to address these challenges by leveraging FPGA’s reconfigurability and specialized components. AutoGNN adapts to diverse graph inputs, efficiently performing computationally intensive tasks such as graph conversion and sampling. By utilizing components like adder trees, AutoGNN executes reduction operations in constant time, overcoming the limitations of serialization and synchronization on GPUs.

AutoGNN integrates unified processing elements (UPEs) and single-cycle reducers (SCRs) to streamline GNN preprocessing. UPEs enable scalable parallel processing for edge sorting and unique vertex selection, while SCRs efficiently handle sequential tasks such as pointer array construction and subgraph reindexing. A user-level software framework dynamically profiles graph inputs, determines optimal configurations, and reprograms AutoGNN to handle varying workloads. Implemented on a 7nm enterprise FPGA, AutoGNN achieves up to 9.0 \times and 2.1 \times speedup compared to conventional and GPU-accelerated preprocessing systems, respectively, enabling high-performance GNN preprocessing across diverse datasets.

I. INTRODUCTION

Graph Neural Networks (GNNs) have garnered substantial attention from both industry and academia due to their impressive accuracy across diverse applications [52], [91], [101]. GNNs achieve superior accuracy over other deep learning methods by effectively learning the features represented by graph vertices and edges, along with their interrelationships [45], [77]. This capability has made GNNs promising solutions for recommendation systems [35], [50], [83], social networks [23], [24], [32], and knowledge graphs [64], [90], [98]. GNNs integrate graph processing and deep learning operations into a unified learning process, enabling them to handle non-Euclidean data structures [7], [40], [84]. However, this combination results in inefficiencies when using conventional processing units like CPUs or GPUs [25], [79]. To mitigate this, numerous hardware acceleration techniques and system framework designs have been introduced. Hardware approaches typically address these inefficiencies by i) designing domain-specific accelerators that combine vector and systolic arrays [87] or ii) utilizing heterogeneous distributed systems incorporating CPUs and GPUs [10], [96], [100]. Meanwhile, system-oriented studies offer frameworks to support parallel execution of GNN processing and deep learning tasks [18], [61], [81] via user-friendly programming models [25], [79].

Despite these substantial advancements, GNNs remain challenging to deploy in real-world systems due to low service performance. Specifically, we find that preprocessing overhead

for large graph datasets accounts for 90.8% of the total GNN service time from an end-to-end perspective (cf. Section III). GNN preprocessing primarily involves *graph conversion* and *graph sampling*, which pertain to transforming the format of the graph dataset and generating a subset of the input graph, respectively. GNN preprocessing is critical in GNN services; without it, *node explosion* can increase the computing demands exponentially [15], [31], [88], [93], preventing the system from meeting service-level latency agreements (SLAs) in real-world inference. Although some studies propose efficient graph formats or sampling algorithms, the preprocessing overhead itself remains to be addressed in the GNN research domain.

We propose *AutoGNN*, a fully automated preprocessing hardware designed toward enhancing GNN inference performance. AutoGNN executes the entire preprocessing workflow, from start to finish, directly in hardware, producing a subgraph optimized for use by GPUs or other GNN accelerators. In this work, we design AutoGNN within an FPGA environment to leverage two essential aspects of GNN preprocessing. First, the computational load in GNN preprocessing varies significantly with the characteristics of the input graph. For instance, graphs with numerous relationships require substantial computation for graph conversion, while preprocessing for smaller-scale data is often dominated by graph sampling tasks. Second, GNN preprocessing involves extensive result reduction processes with complex synchronization operations (e.g., locks and atomic transactions). Unfortunately, this often forces GNN preprocessing into a serialized execution, making it challenging to process efficiently on general-purpose GPUs. FPGAs are well-suited to handle these computational dynamics by adapting to varied graph inputs and efficiently executing reduction operations. Its specialized components, such as adder tree logic, enable result reduction in $\mathcal{O}(1)$ time, significantly improving preprocessing performance.

AutoGNN specifically comprises *Unified Processing Elements* (UPEs) and *Single-Cycle Reducers* (SCRs). The UPE is designed to perform two graph-specific operations – edge sorting and unique vertex selection – within a single hardware logic, each operation corresponding to graph conversion and sampling, respectively. Since each UPE can handle both edges and vertices through shared hardware logic, AutoGNN can scale with multiple UPEs based on input graph demands. This design maximizes FPGA resource utilization, achieving a high level of parallelization and bandwidth efficiency with limited resources. In contrast, SCRs handle the non-parallelizable tasks in both graph conversion and sampling,

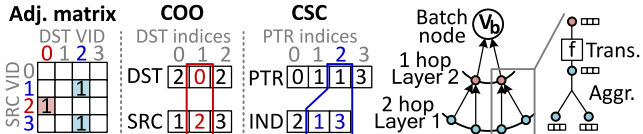


Fig. 1: Graph representation. Fig. 2: GNN inference.

further optimizing GNN preprocessing efficiency.

We also provide user-level software that identifies the characteristics of GNN preprocessing by capturing the dynamics of the input graph. Based on this analysis and a cost function, the software determines the optimal hardware configuration and reprograms the underlying AutoGNN accordingly. We implemented all hardware modules of AutoGNN on a 7nm enterprise FPGA evaluation board and evaluated end-to-end GNN processing to explore the design space with various system configurations. Evaluation results show performance improvements of 9.0 \times and 2.1 \times compared to conventional and GPU-accelerated preprocessing systems, respectively.

The main contributions of this paper are as follows:

- *Comprehensive analysis and characterization of GNN preprocessing.* Although GNN preprocessing is the most time-consuming component in GNN services, there is a lack of research on the specific tasks within this process and their performance bottlenecks. In this study, we break down GNN preprocessing into distinct tasks, examining them both qualitatively and quantitatively. Our in-depth analysis classifies these tasks into parallelizable and non-parallelizable categories, enabling targeted acceleration strategies within a single preprocessing hardware architecture.
- *Unified hardware design for parallelizable tasks.* We reveal that edge sorting and unique vertex selection in GNN preprocessing can be efficiently addressed using prefix-sum [9], [34] and routing [2], [49] algorithms. In addition, we observe that both algorithms can be combined to support set-partition operations [8], [46], which involve extracting data to form a set that meets given conditions. Leveraging these characteristics, we design UPEs, each capable of executing parallelizable tasks within a single hardware architecture. This unified approach maximizes hardware resource utilization, thereby enhancing computing bandwidth.
- *Acceleration of non-parallelizable tasks.* Graph conversion and sampling in GNN preprocessing often require counting specific vertices or edges, tasks that are typically handled serially or with mutual exclusion. To overcome this limitation, we design the SCR with multiple comparator logic, enabling parallel comparisons across numerous inputs. The SCR then aggregates these results using an adder tree or a filter tree, performing vertex or edge counting in a single cycle. By deploying SCRs alongside UPEs in configurations tailored to the input graph's requirements, AutoGNN autonomously executes the entire preprocessing workflow with high efficiency.
- *Reconfigurable design for dynamic graphs.* While UPEs and SCRs are optimized for efficient hardware utilization, the resource demands of GNN preprocessing can vary significantly with graph characteristics. A fixed configuration may not always provide optimal performance. To address this, we implement a cost model that evaluates hardware configurations and graph features to identify the optimal balance of UPEs and SCRs. AutoGNN dynamically reconfigures the FPGA at runtime only when the model determines it is necessary. To

minimize reconfiguration overhead, we analyze each parameter's impact on reprogramming area and latency, allowing it to update only the essential hardware modules selectively.

II. BACKGROUND

A. Elements of GNN Processing and Service

Graph representation. The basic graph representation is the adjacency matrix, where row and column indices represent source and destination *vertex identifications* (VIDs), respectively. Each element indicates whether the two corresponding vertices are connected (1) or not (0), resulting in a matrix with many zero entries, which is inefficient [20], [38]. To enhance the practicality of adjacency matrices in graph processing, various optimized formats have been developed [36], [79]. This section briefly introduces two common representations: *coordinate format* (COO) and *compressed sparse column* (CSC), as shown in Figure 1. The COO format, often called an edge array, stores each edge as a pair of source VID and destination VID, all in an unsorted manner [1]. In contrast, CSC is a vertex-centric structure enabling efficient access to edges associated with a particular node [67], [97]. For example, with a given destination VID, CSC can quickly identify all connected source nodes, retrieving all edges associated with that destination. As shown in Figure 1, CSC consists of two arrays: pointers and indices. The *pointer array*'s indices correspond to the columns of an adjacency matrix (or destination VID), with each value indicating the start offset in the index array. The *index array*, in turn, contains row indices (or source VID). To retrieve all source VIDs connected to a destination VID, one can simply access the range of elements in the index array, starting from the offset of the pointer array up to the next pointer. While COO is suitable for frequently updated graphs, CSC provides efficient graph traversal.

Neural network processing with graphs. In graph theory, transitioning from one node to another via an edge is referred to as a *hop* [19], [101]. A GNN is composed of multiple layers, each representing the one-hop neighborhood of a vertex. These neighborhoods encompass the nodes directly connected to a given *batch node*, which acts as the starting point for inference. To infer features of the batch node, the GNN aggregates the embeddings of neighboring nodes in each layer during an *aggregation* step. The combined embedding is then passed through a conventional deep neural network (DNN), which transforms it to a representation for the next hop (called a *transformation* step). This aggregation-transformation cycle is repeated for all layers, enabling GNNs to learn not only the node and edge information but also the relationships between them [87], [89]. This allows GNNs to achieve higher accuracy than traditional DNNs [31], [45], [77].

Figure 2 shows an example graph spanning two GNN layers and the corresponding inference process, respectively. The inference begins with the layer farthest from the batch node (V_b), represented as the 2-hop layer (layer 1). For each layer, the embeddings of neighboring nodes are aggregated into a single embedding. This aggregated embedding is then transformed into a new representation for the next layer using a function f . For the last layer (layer 2), the transformation is typically performed through a multi-layer perceptron (MLP), generating a new embedding that captures all relationships within the

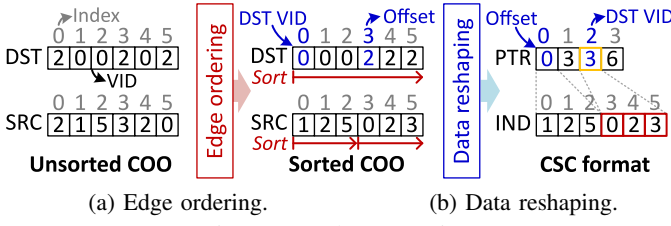


Fig. 3: Graph conversion.

subgraph around the batch node. This final embedding serves as the inference result.

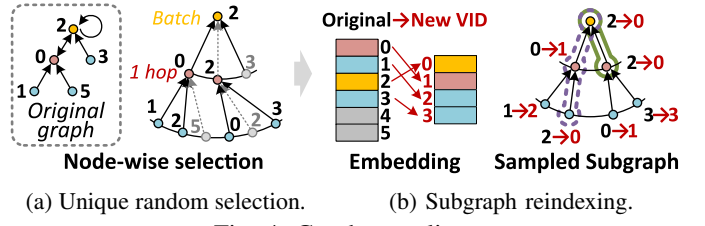
GNN preprocessing for inference. Most graph traversals in GNN services depend on identifying destination nodes from source nodes, making CSC format preferable for efficient traversal. However, raw or application-specific graphs are often stored in COO format for storage efficiency and graph update flexibility [1], [13]. As a result, converting graphs from COO to CSC format is an essential preprocessing step before inference [63]. This *graph conversion* is one of the most time-consuming tasks in GNN preprocessing. Another crucial task in GNN preprocessing is *graph sampling* [42]. Growing graph datasets require substantial memory and increase inference latency. Specifically, as the number of layers and node degree increase, the number of nodes that GNN must explore grows exponentially, a phenomenon known as *node explosion* [21], [75]. The problem amplifies if a node with a high degree (number of neighbor nodes) is accessed during traversal. For example, the Movie dataset may require traversing 99% of the total graph for a two-layer GNN, depending on the batch node. Node explosion leads to significant and unpredictable latency increases in GNN inference, limiting its application to autonomous driving [70], high-energy physics [71], and recommendation systems [22], [57]. To mitigate this, studies proposed to sample a subset of the original graph before inference [43], [53], [73]. For instance, [31] samples a fixed number of nodes per hop, which greatly reduces the computation and memory requirements while preserving reasonable accuracy.

B. Decomposition of GNN Preprocessing

Graph conversion and sampling introduce additional operations into GNN services that were not previously required, placing them on the critical path of GNN processing [59]. Graph conversion primarily involves two tasks: *edge ordering* and *data reshaping*, while graph sampling consists of *unique random selection* (uni-random selection) and *subgraph reindexing*. Edge ordering and data reshaping process a large number of graph components, necessitating extensive parallelization to improve efficiency. In contrast, uni-random selection and subgraph reindexing work on a smaller subset of graph elements but require frequent updates and synchronization, making these more complex and computationally demanding.

Edge ordering. Edge ordering facilitates efficient access to nodes based on destination VIDs. It begins by sorting edges primarily by their destination VIDs and then secondarily by their source VIDs, maintaining the order of destinations. This approach ensures that edges sharing the same destination node are grouped sequentially in the result. As shown in Figure 3, this sorted edge array serves as a foundational structure for the CSC format, enhancing the efficiency and performance of graph sampling and aggregation operations in GNN inference.

Data reshaping. While edge ordering produces a sorted COO array, locating all source nodes for a given destination VID



(a) Unique random selection.

(b) Subgraph reindexing.

still requires a binary search. To overcome this, data reshaping repurposes the sorted COO array into an index array, creating range information for each group of edges that share the same destination VID. The pointer array is constructed by scanning the index array sequentially and setting a start offset whenever a new destination VID is encountered. This process is computationally intensive and offers limited opportunities for optimization. We will examine its performance challenges in more detail in the following section.

Unique random selection. This is a critical step in sampling a subgraph and can be performed in two ways: node-wise or layer-wise selection [54], [76]. In node-wise selection (Figure 4a), a batch node selects k neighbors at the first hop, which are iteratively sampled for additional k neighbors across multiple hops to expand the neighborhood. In contrast, layer-wise selection samples k neighbors at each layer without requiring interconnections, completing the process in fewer steps. While layer-wise selection is faster, node-wise selection is preferred for its higher accuracy. Ensuring uniqueness and randomness during the vertex selection process is crucial. Uniqueness prevents redundant selections, preserving the total number of sampled vertices, while randomness improves inference accuracy [31], [58]. This process often involves checking a synchronized dictionary (i.e., map) to track selected nodes.

Subgraph reindexing. After sampling the original graph, the embedding features must be restructured to align with the sampled nodes. As shown in Figure 4b, this involves generating a new embedding table by extracting the embeddings of the sampled vertices from the original embedding table, which is ordered by VIDs. However, since the indices in the sampled embedding table differ from the original VIDs, renumbering these VIDs is required to maintain consistency. Subgraph reindexing addresses this by mapping each original graph VID to a new VID in the sampled subgraph. Although this procedure has lower latency than other GNN preprocessing tasks, the requirement to manage mapping information in a mutually exclusive manner introduces additional delays. Note that while each hop of the uni-random selection ensures newly chosen vertices are distinct, loops in the parent-child relationships may lead to repeated vertices in the final result. Specifically, a vertex can reconnect to itself (highlighted by a solid line) or be revisited after multiple hops (highlighted by a dashed line). Consequently, subgraph reindexing outputs are initially collected in COO format, then undergo edge ordering and data reshaping to produce the final CSC representation of the sampled subgraph.

III. CHALLENGE AND MOTIVATION

A. Analysis of GPU-Augmented Preprocessing

To better understand the overhead imposed by GNN preprocessing, we evaluate 11 real-world graph datasets selected from open-source benchmarks [25], [37], [79]. Table II sum-

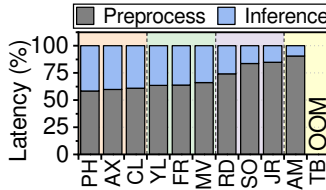


Fig. 5: Analysis of GNN preprocessing overhead.

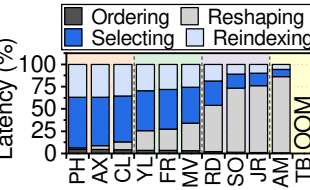


Fig. 6: Breakdown analysis of GNN preprocessing.

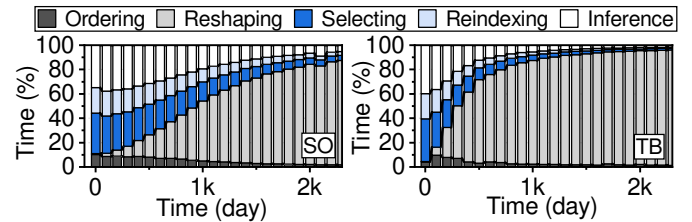
marizes the key characteristics of graph datasets. The preprocessing and inference tasks are executed on an RTX 3090 GPU [65] using DGL [79], a state-of-the-art GNN framework.

Analyzing overhead significance. Figure 5 shows the proportion of GNN preprocessing within the total latency of GNN services. For clarity, workloads from each domain are arranged from left to right in ascending order of edge count. Despite the use of GPU acceleration in DGL to optimize preprocessing, it still accounts for an average of 70% of the total inference time. The figure also reveals that the overhead of GNN preprocessing becomes increasingly significant as the graph size grows. This is because preprocessing load scales proportionally with graph size, whereas inference latency (Inference) remains relatively stable due to graph sampling.

Decomposing the preprocessing latency. Figure 6 breaks down the latency of GNN preprocessing into its four main tasks: edge ordering (Ordering), data reshaping (Reshaping), unique vertex selection (Selecting), and subgraph reindexing (Reindexing). Two key observations emerge from the analysis. First, no single task consistently dominates preprocessing time across all network domains. Second, latency trends vary with the size of the input graphs.

Specifically, for smaller graphs with fewer than 500K edges, graph sampling (Selecting + Reindexing) contributes the most to preprocessing latency, with Selecting and Reindexing accounting for 33.8% and 22.1% of the latency, respectively. However, their contributions decrease by 7.5% and 5.2% as the graph size increases. This reduction occurs because Selecting applies to a limited number of hops, regardless of graph size. In contrast, for larger graphs with edge counts ranging from tens of millions to billions, graph conversion (Ordering + Reshaping) becomes the primary bottleneck. In these cases, Ordering and Reshaping account for 1.8% and 86.1% of the latency, respectively. This shift is due to the need for graph conversion to process the entire graph, both the original graph for sampling and the sampled subgraph for inference.

Considering graph dynamics. Even within a single workload, the latency trends for the four primary preprocessing tasks can change significantly over time. Figure 7 shows GNN service latency for two large datasets, SO and TB, which represent social and e-commerce network domains, respectively. In these domains, user-to-user connections and behaviors are frequently updated, causing the graphs to evolve continuously. For example, the number of edges in each dataset increases by 0.52% and 0.95% per day, respectively, highlighting the dynamic nature of these graphs. As shown in Figure 7, the latency initially is dominated by Selecting within the GNN inference services. Over time, however, this trend shifts. After 400 days (SO) and 20 days (TB), respectively, Reshaping becomes increasingly significant in terms of latency, eventually



(a) Social network (SO).

(b) E-commerce (TB).

Fig. 7: Latency breakdown of dynamic graphs.

surpassing Selecting as the dominant task. This shift occurs because Reshaping must handle the continuously growing number of edges and degrees, while the latency of Selecting remains bounded by the fixed k value. This pattern is consistent across both datasets and underscores the need for adaptable hardware configurations, as no single fixed setup can accelerate all tasks under such dynamic conditions.

B. Removing Preprocessing from Critical Path

To eliminate preprocessing overhead from the critical path of GNN services, AutoGNN accelerates and fully automates all time-consuming tasks in hardware, streamlining the entire preprocessing workflow. This is achieved by *fundamentally redesigning the underlying algorithms to minimize mutual exclusion (atomic) operations in GNN preprocessing, while maximizing parallelization* and acceleration wherever possible. AutoGNN’s efficiency stems from its core design, which incorporates *unified processing elements* (UPEs) and *single-cycle reducers* (SCRs). These reconfigurable components allow for varying logic counts and hardware sizes to accommodate diverse graph preprocessing needs. UPEs efficiently handle edge ordering and unique random selection, while SCRs significantly reduce the latency of data reshaping and subgraph reindexing. Together, these components ensure high performance across a wide range of GNN network domains.

Accelerating Ordering and Selecting. UPE is designed with the insight that both edge ordering and uni-random selection can be implemented using a common operation: extracting elements that satisfy specific conditions and organizing them into a new set [8], [46], called *set-partitioning* in this work. For edge ordering, UPE leverages a characteristic of typical graph datasets: although there are many vertices, their VIDs are integers drawn from a small, contiguous range. We therefore target radix sort, whose digit-wise passes are precisely set-partitioning; this makes it an ideal fit for UPE, and accelerating set-partitioning with UPE directly speeds up radix sort. For uni-random selection, UPE first uses set-partitioning to split the vertices into two buckets, one containing the sampled vertices and the other containing the unsampled vertices. It then repeatedly draws a random vertex from the unsampled bucket only, guaranteeing uniqueness without a full-space scan, thereby improving parallelism and performance.

A key challenge in set-partitioning is determining the new position of each extracted element in the output set. UPE addresses this by integrating two logic blocks: one calculates the cumulative sums for the elements in an array, indicating the distance each element should shift to the left, and the other repositions the elements based on these offsets, all in a single cycle. This enables UPE to partition sets by radix or state (e.g., sampled or unsampled) in just a few cycles. Further details on UPE are discussed in Section IV-C.

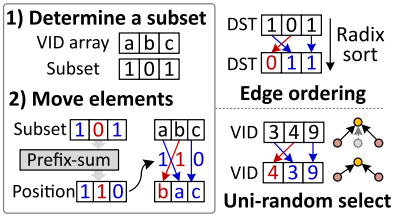


Fig. 8: Set-partitioning.

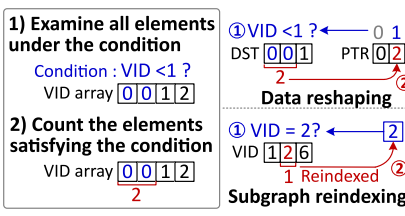


Fig. 9: Set-counting.

Reducing Reshaping and Reindexing. Data reshaping and subgraph reindexing can also be both reduced to a single core operation: counting elements in a set that satisfy a given condition, a process referred to as *set-counting* in this work. The primary challenge in implementing this algorithm lies in its inherently mutually exclusive nature. Updating a counter variable typically requires atomic operations, which severely limit parallelism in these preprocessing tasks. In addition, the processing bandwidth for data reshaping and subgraph reindexing is constrained by the size of the input array and the number of threads available for simultaneous operation.

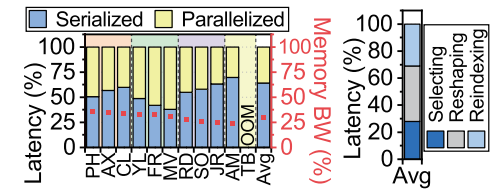
The SCR overcomes these challenges by utilizing thousands of comparators and an adder/filter tree to aggregate the comparator outputs in a single cycle. This architecture enables efficient computation of the range information required for constructing the pointer array in CSC format, thereby significantly accelerating Reshaping. Similarly, SCR identifies specific VIDs in the input, streamlining the creation of an index map and thereby reducing the complexity of Reindexing. Further details on SCR’s design and implementation are discussed in Section IV-C.

IV. HARDWARE-DRIVEN GNN PREPROCESSING

A. Redesigning GNN Preprocessing

Set-partitioning. This is an algorithm that divides a given array of VIDs into two disjoint subsets by evaluating each element, determining its subset, and moving the element accordingly. Instead of scanning all elements, set-partitioning can be efficiently implemented by relocating elements based on prefix-sum results. The prefix-sum operation generates a new array by cumulatively counting elements in the input array that satisfy a specific condition, allowing us to evaluate the position of each element in the new set. Figure 8 shows set-partitioning used in edge ordering and uni-random selection. Each prefix-sum value is the element’s exclusive write index in the output: for edge ordering, it gives the radix bucket offsets, and for uni-random selection, it gives the compact position in the unsampled array. Using these indices, we scatter elements in one pass, streamlining both tasks.

Set-counting. This operation examines all elements in a set against a specified condition and counts the number of elements that satisfy it. As shown in Figure 9, it is applicable to both data reshaping and subgraph reindexing. In data reshaping, the pointer array is constructed based on the result of edge ordering, which consists of arrays for destination and source VIDs. Data reshaping can be viewed as set-counting based on the observation that the index of the pointer array corresponds directly to the destination VID, and the value at each index represents the number of elements with destination VIDs smaller than the index. Thus, set-counting can efficiently populate the pointer array by counting the



(a) Execution breakdown. (b) Serial tasks.
Fig. 10: Serialized computation analysis.

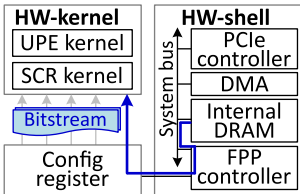
elements that satisfy the condition for each destination VID. Note that a common approach is to increment a counter for the processed edges and update the previous edge’s destination VID while traversing the sorted edge array. However, this requires sequential execution, as each step depends on the previous one. Viewing data reshaping as set-counting effectively enables concurrent computation of each pointer array entry, thus improving throughput.

In subgraph reindexing, the goal is to map the results of uni-random selection to renumbered IDs if they have not been mapped already. The critical step in this process is checking and updating the mapping. While a hash map is typically used for this process [11], resizing the hash map incurs a time complexity of $O(n)$. Set-counting can replace the hash map in this process. Similar to data reshaping, two arrays are maintained: one for the original VIDs (before reindexing) and another for the updated VIDs (after reindexing). By setting the VID from uni-random selection as the condition for set-counting, it can determine whether the VID has been reindexed without relying on a hash map, streamlining the process.

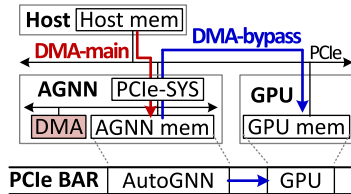
Limits for redesigned algorithms. Although the redesigned algorithms for set-partitioning and set-counting can be accelerated on conventional GPUs, their parallel architectures cannot fully remove GNN preprocessing from the critical path of GNN services. These limitations arise from the need to synchronize shared resources, such as the counter variables and map structures, across multiple GPU threads, which restricts the simultaneous execution of all threads. As shown in Figure 10a, when GNN preprocessing is accelerated on a GPU (RTX 3090) using set-partitioning and set-counting within a CUDA kernel, the execution time is divided into parallelized and serialized portions. As shown in the figure, 64.1% of the overall execution time remains serialized, on average, resulting in low GPU resource utilization. Specifically, only 30.3% of the GPU’s memory bandwidth is utilized on average, negatively impacting performance. Further analysis in Figure 10b shows that uni-random selection, data reshaping, and subgraph reindexing contribute 27.9%, 41%, and 31.1%, respectively, on average, to the non-parallelizable tasks.

B. System Architecture Overview

To overcome these challenges, AutoGNN optimizes set-partitioning and set-counting by minimizing non-parallelizable tasks while maximizing resource utilization on FPGAs through UPEs and SCRs. While FPGAs are generally slower than ASICs, AutoGNN’s hardware design achieves high performance in graph dataset preprocessing by fully exploiting FPGA resources. Its modular architecture, with configurable UPEs and SCRs, allows seamless adaptation to dynamic graphs and varying workloads. In addition, the accompanying software framework enhances flexibility by dynamically



(a) Overall architecture.



(b) AutoGNN interface.

Fig. 11: High-level view of AutoGNN.

adjusting hardware configurations at runtime. By decoupling processing bandwidth from dataset-specific constraints, AutoGNN consistently delivers efficient and robust preprocessing for GNN services across diverse environments.

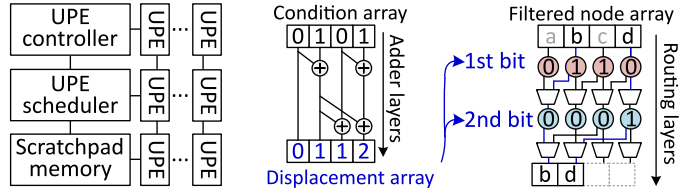
Figure 11a shows the overall architecture of AutoGNN, which comprises two main FPGA components: the hardware kernel (*HW-kernel*) and the hardware shell (*HW-shell*). The HW-kernel is a reconfigurable area containing the UPE kernel and SCR kernel, while the HW-shell is fixed and unaffected by changes in the input graph dataset. The HW-shell includes peripheral components such as the FPGA programming port (*FPP*) controller, for example, ICAP [48], [66], and a PCIe controller. These modules are interconnected via a system bus, allowing the host to reconfigure UPEs and SCRs on the HW-kernel by writing pre-prepared bitstreams from AutoGNN’s internal DRAM to the FPP controller and associated registers.

Figure 11b depicts how AutoGNN interfaces with the host and GPUs (or other types of accelerators). A PCIe-SYS controller serves as the bridge between AutoGNN’s internal system bus and the PCIe interface, exposing two distinct DMA regions: DMA-main and DMA-bypass. DMA-main facilitates data transfer using a PCIe descriptor, which acts as a scatter-gather list to enable AutoGNN to efficiently copy large-scale COO data from the host’s system memory. This is particularly useful for COO datasets that are scattered across system memory but contiguous in userland. In contrast, DMA-bypass supports conventional memory reads and writes via PCIe BAR, functioning similarly to memory-mapped I/O (MMIO). The DMA-bypass is accessible to the host’s software framework, enabling direct mapping to the GPU or other accelerators’ internal memory. This simplifies the transfer of preprocessed, small-sized results, such as subgraphs, to the host or GPU.

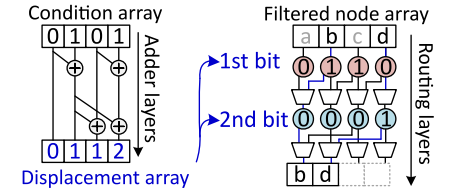
C. Reconfigurable Blocks for Acceleration

UPE kernel design. Figure 12a shows the internal structure of the UPE kernel, consisting of a UPE controller, multiple UPEs, and a UPE scheduler. These components are interconnected via a crossbar switch and share a scratchpad memory. The UPE controller manages input data and intermediate results, storing and retrieving them from the scratchpad memory. To maximize parallelism, the UPE scheduler oversees UPE execution, using a scoreboard to track the status of each UPE (busy or idle) and assign input data accordingly.

Each UPE integrates prefix-sum and relocation logic, and is reconfigurable in its number and size. It processes two input arrays: one for nodes (VIDs) and another for condition values (booleans). The condition array is fed into the prefix-sum logic, which generates a *displacement array*. This array contains cumulative counts of elements in the node array that satisfy the given condition values. Figure 12b provides an example of this logic with four input elements. The prefix-sum logic is implemented as a hierarchical adder network: the



(a) UPE kernel.



(b) Prefix-sum logic.

Fig. 12: UPE kernel design.

first layer computes local sums for the first and second halves of the array, and subsequent layers propagate and combine these sums. The result is a displacement array produced in $O(\log n)$ adder layers. Because the inputs are booleans, each adder only needs a width of $\log n$ bits. We observed that this hardware can process hundreds of elements in a single cycle.

Meanwhile, the node array is processed through AND gates with the condition array, producing a filtered node array where elements that do not meet the conditions are cleared to zero. The displacement array is then fed into the relocation logic, which shifts elements in the filtered node array based on the corresponding values in the displacement array. As shown in Figure 12c, the relocation logic employs $O(\log n)$ routing layers. Each layer decomposes the movement distances of input elements into powers of two and shifts the elements accordingly, moving them leftward at each stage. Note that each multiplexer in the relocation logic has a single-bit select input to choose between two sources for the subsequent layer. The input/output width matches the bit width of the array elements being aligned (64 bits in AutoGNN to store two VIDs). These iterative operations, carried out by the prefix-sum and relocation logic, support various preprocessing tasks such as edge ordering and unique random selection. The UPE controller orchestrates these steps and combines their outputs to complete the desired preprocessing, depending on the specific task or data size.

SCR kernel design. Figure 13a shows the SCR kernel architecture, which comprises two primary controllers: the reshaper (reshaping controller) and the reindexer (reindexing controller). These controllers are connected via a simple bus, such as an AXI crossbar in our implementation, which provides a single port to the HW-shell. This design ensures correct signal timing regardless of the placement of the reshaper and reindexer. The reshaper is equipped with a set of registers to handle the COO format and intermediate results from the underlying SCRs, while the reindexer incorporates an SRAM bank to store the mapping information. Behind the reshaper and reindexer, a reconfigurable number of SCRs are deployed.

Each SCR is composed of two key components: comparator logic and reducer logic. The comparator evaluates all elements of the input array against a given target, while the reducer aggregates the comparison results into a single output. Figure 13b depicts the internal structure of an SCR, which can be configured for either reshaping or reindexing tasks. An SCR receives two inputs: an array and a comparison target. For the reshaper, the comparator subtracts the target from each element of the input array and outputs a positive result if the subtraction is greater than or equal to zero. Note that the comparator must match the bit width of the comparison target (32 bits for a VID). The reducer, implemented as an adder tree, aggregates these results into one value that populates the pointer array in data reshaping. Since the comparator produces 1-bit outputs,

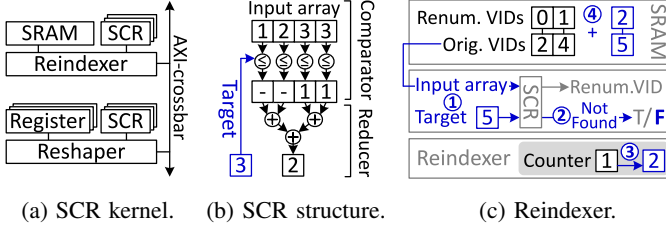


Fig. 13: SCR kernel design.

the reducer requires an adder width of up to $\log n$, where n is the number of concurrently processed elements.

The reshaper receives the sorted COO from the UPE and temporarily stores it in a buffer. It then uses multiple SCR units to determine the frequency of occurrences for the current target VIDs ($v \sim v + n - 1$) within the COO. Subsequently, the reshaper maintains two counters: one for the progress on target VIDs (i.e., the current v), and another for the number of COO elements already consumed. Whenever a target VID meets a COO element with a value strictly larger than itself, the target VID is marked as completed, and v is advanced to the next VID by updating the target counter accordingly. Meanwhile, any COO element with VID smaller than v is marked as consumed, as it can no longer contribute to the remaining targets. On consumption, the reshaper fetches the next COO segment into the buffer and reiterates the counting steps until all COO segments have been processed.

For the reindexer, the hardware design is similar, except that the reducer adopts a filter tree (OR gates) instead of an adder tree. In this case, the inputs represent mapping elements from the SRAM bank and the new VID to be reindexed. As it is required for the reindexer to return the actual value (the reindexed VID), together with an indication of a search hit, the filter tree's bit width must match that of each element being filtered plus one (32+1 bits for a VID). Figure 13c further shows the operation of the reindexer with its associated SCRs and SRAM bank. The reindexer maintains a counter to track the number of mappings completed so far. Two arrays are stored in the SRAM bank: one for original VIDs and another for renumbered VIDs (as described in Section IV-A). For each index pair in these arrays, the SCR checks whether the original VID exists. If it does, the SCR returns the renumbered VID. If not, the reindexer increments the counter, assigns it as the new VID, and stores the input target and the counter value as a new mapping pair in the SRAM. This design ensures high-performance reshaping and subgraph reindexing.

V. DETAILS OF END-TO-END OPERATIONS

A. End-to-End Workflow and Dataflow

Figure 14 shows the end-to-end GNN preprocessing workflow fully automated in hardware. It begins with the COO-to-CSC conversion, initiated by the UPE controller through edge ordering. The edge ordering workflow comprises four steps: concatenation, splitting, merging, and deconcatenation, all executed in parallel by multiple UPEs. Details regarding these steps will be explained shortly. After sorting the COO, the SCR controller (reshaper) generates the pointer array using multiple SCRs, as described in Section IV-C. Independent set-counting allows each pointer to be processed in parallel. After data reshaping, the source nodes associated with each pointer (destination VID) are identified. The UPE controller

then begins unique random selection across source nodes for each pointer, using the same UPEs previously used for edge ordering. This sequential use of shared hardware ensures no UPE remains idle, optimizing FPGA resource usage. Meanwhile, the sampled nodes are managed by the SCR controller (reindexer). As described in Section III-B, the reindexer checks mapping information stored in the SRAM using set-counting and finalizes the sampled graph by renumbering.

Workflow for edge ordering. While UPE has no limit on the number of elements it can process simultaneously, increasing the element count deepens the prefix-sum and relocation logic, degrading performance. To mitigate this, the UPE controller splits the COO format into smaller chunks matching the UPE's processing capacity, referred to as the *UPE width*. It then performs radix sort on these chunks. In our FPGA implementation using VPK180 [4], UPEs can be configured up to 240 instances, each with a width of 64 elements. However, the number of UPEs and their width can scale further depending on the size of the underlying FPGA.

Figure 15 shows the UPE controller's workflow for edge ordering. Since the COO represents edges as pairs of destination VIDs and source VIDs, the UPE controller first concatenates these VIDs for each pair. It then splits the concatenated pairs into chunks based on the UPE width. Each UPE processes a chunk independently, performing radix sort (Section IV-C), resulting in locally sorted COO chunks. To produce a fully sorted COO, the UPE controller employs UPEs to merge these locally sorted segments. By leveraging the UPEs to find the minimum values among the sorted chunks simultaneously, the UPE controller eventually produces a globally sorted COO. Algorithm 1 describes these steps in detail. The merge process starts by reading the smallest $w/2$ elements from each input array, where w is the UPE width (lines 2-3), and sorting them (line 5). Since these are the smallest in both arrays, the first $w/2$ elements of the sorted buffer are returned (line 6). The buffer still holds $w/2$ elements, so the scheduler reads only $w/2$ new elements from either array A or B . To decide which array to read, the scheduler compares the first elements in A and B , then copies $w/2$ elements from the array with the smaller first element (lines 7-9). By repeating this process, arrays A and B can be merged at a rate of $w/2$ elements per cycle. Finally, the UPE controller deconcatenates the sorted elements back into pairs of destination and source VIDs to complete edge ordering.

Control-path of graph sampling. The UPE controller samples graphs by selecting k nodes from the source nodes, ensuring both uniqueness and randomness. Note that for node-wise sampling methods [14], [31], the controller is called for every neighbor array. To support layer-wise sampling methods [15], [39], [88], [102], all neighbor node arrays of a layer are first aggregated together as a single array; the UPE controller is then called for the aggregated array, selecting k nodes per layer. This flexibility can effectively support a wide range of popular GNN models. Figure 16 illustrates a simplified version of this process. First, the controller creates an index array whose length equals the number of source nodes, each element corresponds to the index of the source node. It then repeats the random selection procedure k times. Each iteration draws a new random index from the unsampled set to create a one-hot condition for that index, and let the

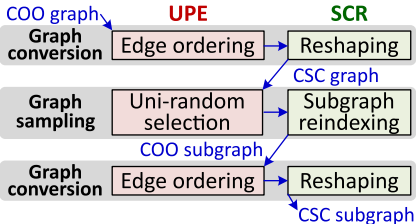


Fig. 14: End-to-end workflow.

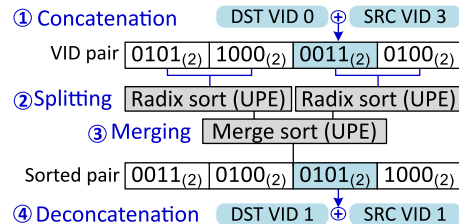


Fig. 15: Workflow for edge ordering.

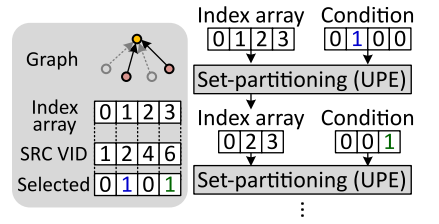


Fig. 16: Graph sampling.

UEs run set-partitioning to extract the chosen element in a single cycle. The UPE controller maintains a bitmap and updates it whenever a new index is extracted by marking the extracted index as sampled, preventing reselection, and thus guaranteeing uniqueness. After k indices are selected, the controller builds a condition array from the bitmap and applies set-partitioning once more on the original source node array to extract the k -sampled neighborhood.

B. Dynamic Reconfiguration and Software

AutoGNN sustains high performance even as graph characteristics shift at runtime by dynamically reconfiguring the accelerator. To remove the long synthesis latency from the critical path, we do not synthesize hardware at runtime, but instead select among a small set of pre-compiled bitstreams.

Bitstream generation. Both UPE and SCR are parameterizable in their count and width. We therefore pre-compile a series of bitstreams that fit the target FPGA. Because both hardware are most efficient when configured with widths that are a power of two, we start from a bitstream consisting of a single large UPE (and SCR), and iteratively halve the width and double the instance count, generating the corresponding RTL and compiling them offline using Vivado. On our VMK180 board, this yields ten UPE variants and ten SCR variants, thus twenty kernel bitstreams in total. Rather than compiling every $UPE \times SCR$ combination, AutoGNN partitions the device into two reconfigurable regions with a fixed area split of 70:30, which was effective in our evaluation (Section VI-B). The static partitioning allows us to pre-compile ten UPE bitstreams and ten SCR bitstreams separately. At boot, all twenty bitstreams (50 MB each, 1 GB total) are staged in the internal DRAM of AutoGNN. This confines the reconfiguration cost to bitstream loading and partial reconfiguration. To this end, the reconfiguration process takes ~ 230 ms, including 3 ms to load the bitstream from DRAM and 225 ms for FPGA reconfiguration through the Xilinx ICAP IP [86] operating at 100 MHz. Note that, because UPE and SCR reside in separate reconfigurable regions, only the region that needs to change could be reprogrammed, roughly halving the reconfiguration overhead.

Algorithm 1: Merge sorting using UPE.

```

1 fn Merge(A and B: sorted edge arrays of length n) ▶ C: the merge
  array
2   a, b, c = w/2, w/2, 0           // current index of A, B, C
3   buf[0 : w/2], buf[w/2 : w] = A[0 : a], B[0 : b]
4   while a < n and b < n do
5     UPE_sort(buf)                // Sort the buffer
6     C[c : c + w/2] = buf[0 : w/2]; c = c + w/2
7     let is_a = A[a] < B[b]
8     buf[0 : w/2] = is_a? A[a : a + w/2] : B[b : b + w/2]
9     if is_a then a = a + w/2 else b = b + w/2

```

Cost function. At runtime, the host collects light-weight graph metadata (e.g., the number of nodes n and edges e) and GNN hyperparameters (e.g., the number of layers l , the max sample count k , and the batch size b). A cost function then estimates the end-to-end latency for each pre-compiled bitstreams to find the best hardware configuration for the specified input graph and GNN model. Specifically, the cost function evaluates three analytic models, each for ordering, selection, and reshaping as shown in Table I. The cost functions are parameterized by the hardware and workload (input graph and GNN model) configuration. The hardware parameters includes the number and width of UPE/SCR engines (n_{upe} , w_{upe} , n_{scr} , w_{scr} , respectively), while the workload parameters include n , e , l , k , and b .

For edge ordering, each UPE processes its assigned chunk independently. Therefore, the runtime is determined by the dividing total work, which is equal to the number of edges (e) multiplied by the number of merging rounds (m), by the aggregated UPE throughput, which scales proportional to the throughput of each UPE ($w_{upe}/2$) and the number of UPEs (n_{upe}). For uni-random selection, each UPE selects one node per step, yielding n_{upe} nodes per step across all UPEs. The runtime is therefore estimated by dividing the total number of nodes selected (s) by n_{upe} , where s is calculated as the product of the batch size (b) and k nodes selected per layer (l). For data reshaping, SCRs process the COO array in parallel to build the CSC pointer array. Time is bounded by the maximum of two terms: the COO-side term, which is proportional to the number of edges (e) divided by the SCR width (w_{scr}), and the CSC-side term, which is proportional the number of nodes (n) in the pointer array divided by the number of SCRs (n_{scr}). Evaluating the cost function consists of two steps: i) evaluating the cost-related graph parameters, which is handled by AutoGNN during graph conversion, and ii) scoring the costs for all available bitstreams, which is done by the host library. In our evaluation, the cost computation took less than 0.1 ms, which is under 0.1% of the end-to-end latency.

Software architecture. We modified the deep graph library (DGL) to integrate AutoGNN into GNN inference services using commodity GPUs (or hardware accelerators). All interfaces remain consistent with DGL, with additional functions for graph management, such as `uploadgraph()`, which is similar to `updategraph()`. To maintain compatibility with DGL interfaces, the implementation details for managing

Task	Cost function
Edge ordering	$m = \log_2 (e/w_{upe}) - 1$ $\text{cycle}_{\text{Ordering}} = \left(\frac{2 \times m \times e}{n_{upe} \times w_{upe}} \right)$
Unique random selection	$s = b \times k^{l+1} - 1$ $\text{cycle}_{\text{Selecting}} = s/n_{upe}$
Data reshaping	$\text{cycle}_{\text{Reshaping}} = \max \left(\frac{n}{n_{scr}}, \frac{e}{w_{scr}} \right)$

TABLE I: Cost functions of GNN preprocessing tasks.

	Category	#Edges	#Nodes	Deg	Category	#Edges	#Nodes	Deg	
Citation Network	Physics [79] (PH)	495K	34.5K	14.4	Social Network	Reddit2 [25] (RD)	23.2M	233K	99.6
	arxiv [37] (AX)	1.16M	169K	6.84		StackOver [51] (SO)	63.5M	6.02M	10.5
	collab [37] (CL)	2.36M	236K	10.0		Journal [51] (JR)	69.0M	4.85M	14.2
Interaction Network	Yelp [79] (YL)	6.81M	46.0K	148	E-commerce Network	Amazon [37] (AM)	123M	2.45M	50.5
	Fraud [79] (FR)	7.13M	11.9K	597		Taobao [3] (TB)	400M	230K	1744
	Movie [79] (MV)	11.3M	3.71K	3052					

TABLE II: Important characteristics of dataset.

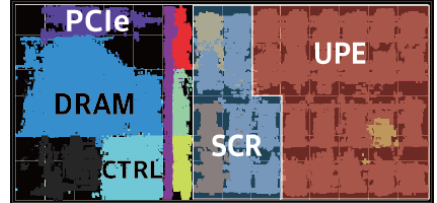


Fig. 17: Floorplan.

AutoGNN are abstracted behind two software components: AutoGNN’s user-level library (AGNN-lib) and kernel driver (AGNN-drv). AGNN-lib is responsible for i) managing graph I/O, ii) determining hardware reconfiguration, and iii) interacting with AutoGNN for preprocessing tasks.

Although graph datasets are smaller than their embeddings, they are large enough to be scattered in user memory (e.g., GB-scale). To handle such graphs, AGNN-drv utilizes AutoGNN’s DMA-main interface through `pci_ioremap_bar()` [82] and processes them using a scatter-gather list [62]. AGNN-drv creates a PCIe descriptor for the scatter-gather list based on the given graph data and writes the descriptor address to DMA-main. AutoGNN then retrieves the graph dataset by referencing the descriptor and preprocesses it. Unlike the GPU, which must deallocate the graph datasets during the model inference process, AutoGNN can store the previous graph data within device memory. This enables AutoGNN to only read the updated portions of the graph from the host, minimizing data transfer overheads. Instead, AutoGNN requires an additional data movement to transfer the preprocessed graph to the GPU. However, since the preprocessed graph is already sampled, its size is substantially smaller than the original graph, making this overhead negligible. In typical GNN scenarios, this transfer latency is approximately 2.8 ms, accounting for less than 1% of the total end-to-end GNN latency.

AGNN-lib evaluates the cost function if the current hardware configuration is suboptimal due to changes in the graph. If the latency exceeds the threshold, AGNN-lib selects the optimal pair of hardware profiles (one for UPE, one for SCR) and sends its key to AutoGNN. The AutoGNN’s hardware shell, specifically the FPP controller, uses this key to locate the bitstream’s address in the internal DRAM memory and DMA it to the ICAP IP to complete the reconfiguration.

VI. EVALUATION

Prototype. We constructed an AutoGNN hardware prototype implementing modules in RTL and synthesizing them onto a 7nm Xilinx VPK180 FPGA [4]. Figure 17 shows the example

Evaluation System	CPU	Xeon 12-core 512GB, DDR5
	GPU	RTX 3090
	FPGA	VPK180 (4.1M LUT)
Software Configuration	Framework	DGL 2.3.0
	GNN Model	2-layer GraphSAGE
	Selecting k	10
Hardware Configuration	Inf. Nodes	3000
	SCR Resource	30%
	SCR Slots	1
	UPE Width	64

TABLE III: Evaluation setup.

Operation	Algorithm
Ordering	Radix Sort [2]
Reshaping	Histogram Hashing [41]
Selecting	Reservoir Sampling [78]
Reindexing	Histogram Hashing [41]

TABLE IV: Algorithms.

floorplan of our hardware, configured with eight SCR modules and 32 UPE modules respectively. It is connected to a host system with a 128-core Xeon CPU and an RTX 3090 GPU, also used for the compared CPU and GPU-based systems.

Tested model and workloads. We employed a 2-layer GraphSAGE model [58], which selects 10 neighboring samples for each node during preprocessing (i.e., k is set to 10) and uses the resulting 2-hop subgraphs for inference. We selected 11 graph datasets from OGB [37], DGL [79], and PyG [25]. These datasets can be categorized into four groups based on their domains and characteristics: (i) *Citation networks* represent relationships between papers by modeling papers as nodes and citations as edges. These networks typically have small sizes and degrees. (ii) *Interaction networks* express relationships between movies or restaurants by modeling them as nodes and their reviews as edges, resulting in high connectivity. (iii) *Social networks* are graphs that represent relationships between individuals or organizations, which are typically large and exhibit medium connectivity. (iv) *E-commerce networks* are graphs that model customers or products as nodes and purchases or searches as edges, which are typically large. Table II summarizes important characteristics of the datasets.

Compared systems and configurations. We compared seven systems: four baselines and three versions of AutoGNN. Among the baselines, CPU and GPU perform preprocessing on the CPU and GPU, respectively. Both use the DGL [79] framework, and the specific algorithms for each preprocessing step are summarized in Table IV. We also evaluated two configurations that accelerate the graph sampling process. GSamp [28] deploys matrix-centric APIs compiled via a data-flow IR with fusion and super-batching. FPGA [29] utilizes a stream-based sampler logic backed by HBM. Since the accelerator implements sampling only, we run graph conversion on the GPU. The other three systems are our AutoGNN variants, all of which execute end-to-end GNN preprocessing on the FPGA. They differ in how the UPE region is organized for the two stages (ordering and selection) and whether the hardware kernels are reconfigurable. In AutoPre, the UPE region is statically split into two fixed sub-engines: an ordering-only UPE and a selection-only UPE, each provisioned with equal LUT budgets. This design deliberately forgoes the UPE’s unification capability by keeping both stage-specific datapaths, but the two stages still execute serially due to dependencies. StatPre utilizes the whole UPE region in a time-multiplexed manner across ordering and selection. Reusing the UPE, which utilizes most (70%) of the FPGA resources, improves overall resource utilization compared to AutoPre. DynPre additionally leverages partial reconfiguration to adapt the UPE and SCR components to the target dataset at runtime. Unless otherwise noted, the hardware settings of AutoPre and StatPre are fixed and tuned for the MV dataset (an intermediate-sized graph) for best average performance. After preprocessing, all

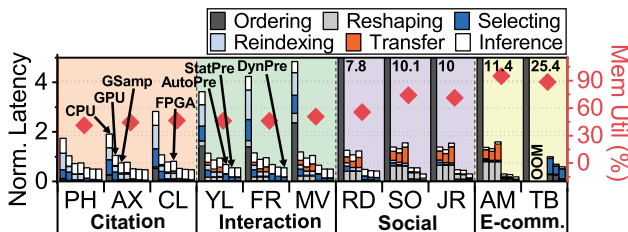
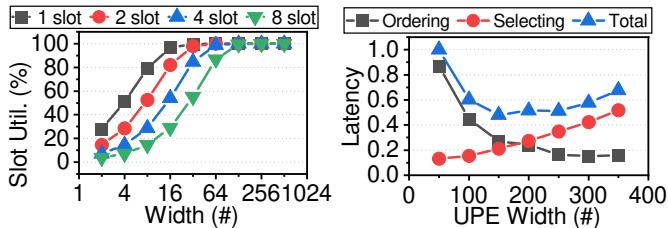


Fig. 18: End-to-end latency.

systems perform GNN inference on the GPU. Table III lists the key software and hardware configurations.

A. Overall Performance

End-to-end latency. Figure 18 compares end-to-end GNN inference latency normalized to GPU. Compared to CPU, the GPU, GSamp, FPGA, AutoPre, StatPre, and DynPre systems reduce overall latency by $3.4\times$, $4.5\times$, $4.1\times$, $7.3\times$, $8.4\times$, and $9.0\times$, respectively. GPU delivers a large speedup for edge ordering by $3421\times$ compared to CPU thanks to its massive parallelism. However, other GNN preprocessing operations exhibit heavy atomic operations which limit GPU performance. Consequently, the end-to-end speedup of GPU over CPU averages only $3.4\times$ on average. GSamp and FPGA further accelerate sampling by $7.5\times$ and $12\times$, respectively. Unlike GSamp, because FPGA implements sampling only, other stages of the GNN, including graph conversion, must run on the GPU. This necessitates the transfer of the full graph between the GPU and the FPGA. The resulting data movement accounts for 24.7% of the end-to-end latency, on average. In contrast, AutoPre automates all preprocessing to the FPGA, so only the graph updates are exchanged with the host. This reduces the transfer overhead by $19.2\times$ and $35.4\times$, on average, compared to GPU and FPGA. Further analysis regarding the transfer overhead is explained through Figure 20. Additionally, AutoPre utilizes SCRs to accelerate reshaping and reindexing, which require atomic operations. To this end, although AutoPre’s per-stage throughput for ordering and selecting can be lower than FPGA, AutoPre can still provide $1.9\times$ performance boost, on average. StatPre improves upon AutoPre by unifying the UPE region; the same UPE module is time-multiplexed across ordering and selection, which raises overall resource utilization. This shortens the end-to-end latency by 14% , on average. DynPre enables partial reconfiguration within the UPE/SCR region, adapting the hardware to each dataset at runtime. This further reduces the end-to-end latency by 21.6% on average. The gains of DynPre are most pronounced for large or low-degree graphs, which differ substantially from MV, where the preprocessing time drops by 53.6% .



(a) SCR width (AX).

(b) UPE width (AM).

Fig. 23: Optimal hardware configuration.

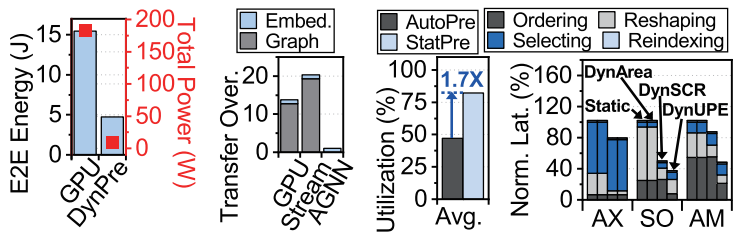


Fig. 19:
Power.

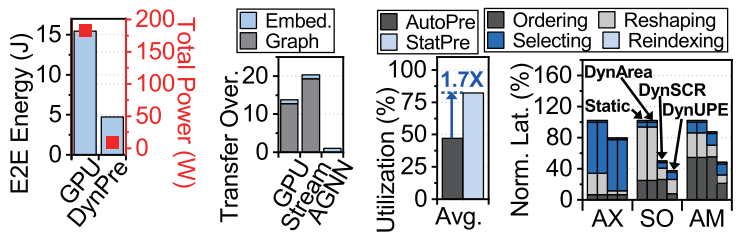


Fig. 20:
Transfer.

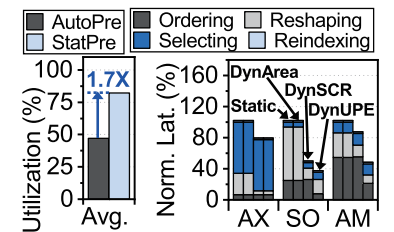


Fig. 21:
LUT
utilization.

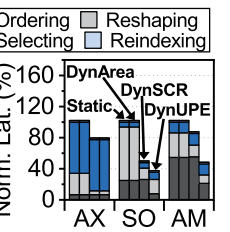


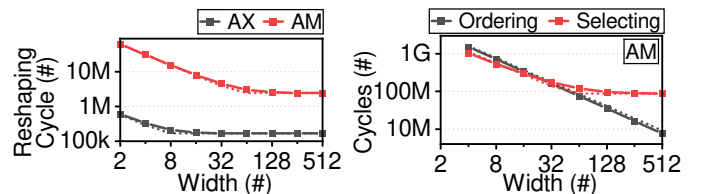
Fig. 22:
Dynamic
reconfiguration.

Memory bandwidth utilization. The right y-axis in Figure 18 reports the memory bandwidth utilization of DynPre. AutoGNN sustains an average utilization of 59.8% , noticeably higher than the GPU baseline (30.3% on average). This gap stems from AutoGNN’s specialized datapaths. UPE and SCR implement prefix-sum and reduction logic with pipelined adders and adder trees, respectively, replacing serialized atomic operations with single-pass kernels. The memory utilization increases with graph size. Larger graphs tend to have long latencies for reshaping, which processes sorted COO segments sequentially; with SCR, each COO segment is consumed in a single cycle, allowing the SCR to fully saturate the memory interface. Consequently, we observe an average utilization of 91.6% on e-commerce graphs.

Power and energy. Figure 19 compares AutoGNN (DynPre) and GPU in terms of power and total energy. During preprocessing, DynPre draws only 9.3W on the FPGA, whereas GPU dissipates 183W for the same workload, yielding a $19.7\times$ lower power draw for preprocessing. When considering end-to-end GNN inference, both configurations execute the GNN model on the GPU, which narrows the energy gap. Even so, thanks to the latency reduction of DynPre, the total energy consumption is on average $3.3\times$ lower than GPU.

B. Detailed Analysis

Transfer overhead. Figure 20 shows the average transfer overhead for GPU, FPGA, and AutoPre. AutoPre reduces transfer overhead by $13.6\times$ and $20\times$ compared to GPU and FPGA, respectively. This stems from AutoGNN’s ability to perform end-to-end preprocessing entirely on the accelerator. For GPU, the same device must handle both preprocessing and GNN model execution. Due to the lack of GPU’s internal memory, the entire graph must be fetched from the host again before each preprocessing pass. For FPGA, on top of the host-GPU transfers, an additional transfer is required to move the CSR-form of input graph produced by the GPU-side graph conversion. In contrast, AutoPre executes all preprocessing stages on a single accelerator and therefore only receives the incremental graph updates from the host. After preprocessing, the resulting sampled subgraph is sent to the GPU for model execution; however, this subgraph is much smaller than the



(a) Accuracy of SCR cycle.

(b) Accuracy of UPE cycle.

Fig. 24: Accuracy of the cost model.

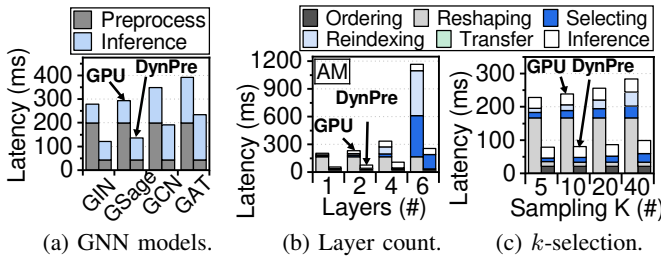


Fig. 25: Diverse GNN model support.

original graph ($1230\times$ on average), so the residual transfer overhead is minimal (0.6% of end-to-end latency).

LUT utilization. Figure 21 compares the average LUT utilization of AutoPre and StatPre. AutoPre forgoes UPE unification and statically partitions the UPE region into distinct accelerators. Because data dependencies force serial execution, the average LUT utilization is only 47%. StatPre improves utilization to 82.2% ($1.7\times$ over AutoPre) by time-multiplexing the same UPE modules across ordering and selection.

Analysis of hardware reconfiguration. To evaluate hardware reconfiguration impact on performance enhancement, we implement three versions of DynPre and compare them with StatPre. DynArea uses an optimal resource distribution between the SCR and UPE modules for each dataset. Compared to DynArea, DynSCR optimally configures the SCR module by optimizing its width and slot count. Compared to DynSCR, DynUPE optimizes the configuration of the UPE module in terms of width and count. In this evaluation, we use three graph datasets as representatives: AX, SO, and AM.

Figure 22 compares the preprocessing latency of StatPre, DynArea, DynSCR, and DynUPE for the three datasets; the latency values are normalized to StatPre. Compared to DynArea, StatPre assigns 30% of the total LUT resources to the SCR module for every dataset, showing that adjusting the balance between the SCR and UPE modules brings negligible performance benefits. This analysis leads to fixing the SCR and UPE module resource distribution at 30:70. Recall that this decision significantly reduces reconfiguration overhead (Section V-B). Next, compared to DynArea, DynSCR reduces the preprocessing latency of AX, SO, and AM by 23%, 51%, and 15%, respectively. This indicates that the optimal configuration of the SCR module for all three datasets is distinct from that in MV. Figure 23a further depicts the slot utilization under varying widths and counts for AX. Basically, slot utilization increases as slot width increases, since the number of edges read per cycle also increases; however, it does not further increase beyond a certain slot width, since the number of nodes recognized per cycle is limited by the slot count. To this end, for AX, which has a small degree, it is more beneficial to increase the number of slots. Lastly, DynUPE reduces the preprocessing latency of SO and AM by 13% and 39%, compared to DynSCR. Figure 23b shows the times for ordering and selecting operations as well as the total time under varying UPE widths and numbers, which highlights how the optimal UPE configuration is determined.

Accuracy of cost model. Figure 24 compares cycles consumed (solid lines) with cycles estimated by our cost model (dotted lines) during preprocessing. Figure 24a shows consumed and estimated cycles in the SCR module under varying slot widths for AX and AM, with a fixed SCR slot count.

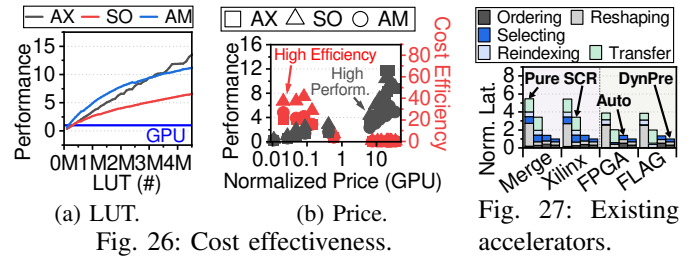


Fig. 26: Cost effectiveness.

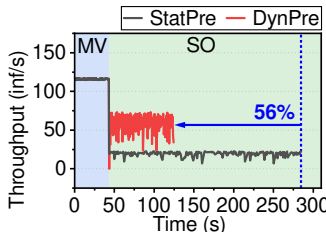
Our model achieves 98% accuracy and captures each dataset’s saturation. Figure 24b plots cycles for ordering and selecting in the UPE module with varying UPE widths for AM. Our model achieves 94% accuracy and effectively captures saturation, enabling identification of an optimal UPE configuration.

Sensitivity on model parameters. Figure 25 illustrates the end-to-end latency of GPU and DynPre with variations in the GNN model (Figure 25a), the number of layers (Figure 25b), and the neighbor sampling parameter k (Figure 25c), for the AM dataset. We analyzed four distinctive models – GIN [80], GraphSAGE [31], GCN [45], GAT [77] – ordered by computational intensity. As the model complexity increases, the portion of GNN preprocessing decreases, narrowing AutoGNN’s relative advantage. Nevertheless, even for the most demanding model (GAT), preprocessing still accounts for 51% of the end-to-end latency, and DynPre delivers a $1.67\times$ speedup over GPU. AutoGNN can also support a wide range of GNN hyperparameters. Increasing the number of layers from one to six increases the inference and sampling latency by $4.1\times$ and $51.1\times$, respectively. Consequently, the overall preprocessing overhead increases, boosting DynPre’s relative speedup from $3.7\times$ to $4.5\times$. Similarly, increasing k amplifies the sampling latency by $2.5\times$, and DynPre’s performance gain over GPU reaches $2.6\times$ due to its streaming, contention-free sampler.

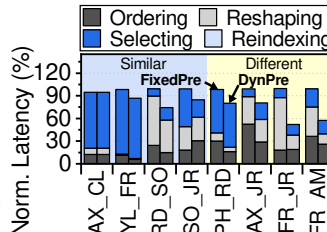
Sensitivity on LUT and price. Figure 26 evaluates the relative performance of DynPre, compared to GPU, while varying the total LUT count (Figure 26a) and using different FPGA boards in a wide price range (Figure 26b). As the LUT count increases from 400K to 4M, the relative performance rises from $1.9\times$ to $9.6\times$ on average. Given that the 3090 GPU has similar costs to a Xilinx FPGA with 400K LUTs [5], FPGA-based preprocessing achieves a $1.9\times$ speedup at an equivalent cost. We further analyzed the performance and cost effectiveness (the performance divided by the price) of AutoGNN on various FPGA boards. On low-price FPGAs, AutoGNN shows moderate speedup against GPU ($1.2\times$ on average), but provides high cost effectiveness ($21.8\times$ on average). On high-price FPGAs, AutoGNN’s cost effectiveness falls; lying between $1.67\times$ and $0.55\times$, but the speedup rises to $7.6\times$ on average. To this end, AutoGNN’s flexible hardware design enables consumers to choose the target FPGA based on their priority: if they want cost effectiveness, a low-end FPGA will suffice; if they lean toward compute power, a high-end FPGA provides greater performance than GPUs.

Other accelerators. Figure 27 shows the relative performance of existing accelerators. We evaluate four designs: two for ordering (merge-sort [72] and insertion-sort [6] accelerators), and two for selection (a stream-based FPGA sampler [30] and precomputation and vector quantization [33]). We evaluate three configurations for each accelerator: i) Pure, which uses the accelerator alone and occupies 100% of the FPGA; ii) SCR,

Fig. 27: Existing accelerators.



(a) Time-series analysis.



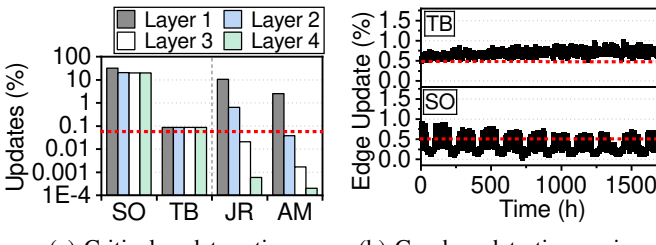
(b) Various graph pairs.

Fig. 28: Consecutive inference using diverse graphs.

which partitions the FPGA 30:70 and adds AutoGNN’s SCR unit to the 30% region; and iii) Auto, which subdivides the 70% region and adds AutoGNN’s UPE to one half to enable end-to-end preprocessing (akin to AutoPre). The final bar is DynPre. SCR, Auto, and DynPre deliver 1.7 \times , 3.3 \times , and 4.5 \times speedups over Pure, respectively. Pure accelerates only one stage (ordering or selection), so overall performance is bounded by the remaining stages and by large transfer overheads. SCR speeds up most preprocessing via the added SCR, but still incurs high transfers due to repeated host-GPU-FPGA handoffs. Auto eliminates those transfers by performing end-to-end preprocessing on the FPGA, yet, like AutoPre, splits the UPE region into ordering and selection-only sub-engines, lowering LUT utilization and capping performance.

Graph update. Figure 29 summarizes two views: i) the minimum graph-update ratio that perturbs GNN outputs while varying the number of layers (Figure 29a), and ii) a time-series of per-hour update ratios for two representative dynamic graphs, TB and SO. On average, 0.74% of the graph changes every two hours, implying that frequent graph reconstruction is required to maintain high GNN accuracy.

Consecutive diverse graphs. Many applications require real-time inference on diverse graphs that vary over time. Figure 28a illustrates a scenario where two distinct graphs, MV and SO, arrive sequentially. StatPre, which utilizes only the optimal configuration of the first graph, experiences a significant throughput drop during SO preprocessing. This is because the graphs have distinct optimal configurations due to MV’s large graph degree. DynPre reconfigures the hardware, which, although it adds a 0.23 second latency, boosts throughput by 2.9 \times thereafter. As a result, DynPre reduces the overall preprocessing time by 56%. Figure 28b further



(a) Critical update ratio.

(b) Graph update time-series.

Fig. 29: Update of dynamic graphs.

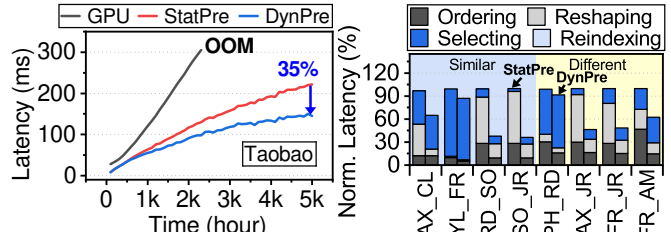


Fig. 30: Dynamic graph.

Fig. 31: Mixed edges.

evaluates when a pair of similar/different graphs is input. Compared to StatPre, DynPre reduces the preprocessing latency of similar and different datasets by 14.6% and 46.1%. This highlights the hardware reconfiguration capability of DynPre, beneficial in scenarios where the graphs vary.

Dynamic graphs. Interactions in a social graph (SO) or item purchases in an e-commerce graph (TB) are often added over time. Figure 30 shows TB’s end-to-end latencies, while edge count and degree increase by 112 \times and 9.2 \times , respectively, over time. The performance benefits of StatPre over GPU become more pronounced, since preprocessing latency occupies a larger share over time. Compared to StatPre, DynPre further reduces the end-to-end latency by 35% by adapting the optimal hardware configuration.

Mixed edges. To evaluate concurrent inferences on two different graphs, we mix edges from graphs within the same category and across different categories. Figure 31 shows the preprocessing latency of these mixed edges under StatPre and DynPre. Compared to StatPre, DynPre reduces preprocessing latency by 98.9% for same-category graph mixes and by 74.1% for cross-category graph mixes.

VII. RELATED WORK

Numerous accelerators have been proposed to reduce GNN processing latency, including GPU-based frameworks [74], [85], FPGA-based implementations [17], [27], [55], [92], [94], [95], and domain-specific ASIC designs [12], [44], [56], [87]. These works focus on GNN inference while ignoring the preprocessing overhead. Although some accelerator works target sorting [16], [47], [60], [68], format processing [69], or sampling [52], they devote most resources to a single function, thus unsuitable for end-to-end GNN preprocessing. In contrast, AutoGNN accelerates preprocessing with reconfigurable unified PEs, achieving high performance across various graphs.

VIII. CONCLUSION

AutoGNN is an FPGA-based accelerator addressing bottlenecks in GNN preprocessing. Leveraging reconfigurable hardware and specialized components, AutoGNN accelerates tasks such as graph conversion and sampling. Our software framework ensures adaptability to varying workloads, optimizing performance in real-time. Implemented on a 7nm enterprise FPGA, AutoGNN delivers up to 9.0 \times and 2.1 \times speedup compared to conventional GPU-accelerated systems.

IX. ACKNOWLEDGEMENTS

The authors thank anonymous reviewers of ISCA’25, MICRO’25 and HPCA’26 for their constructive feedback. This work was supported by Samsung Research Funding & Incubation Center for Future Technology of Samsung Electronics under Project Number SRFC-IT2302-05. This work is protected by one or more patents. Myoungsoo Jung is the corresponding author.

REFERENCES

[1] S. Abi-Karam, Y. He, R. Sarkar, L. Sathidevi, Z. Qiao, and C. Hao, "Gengnn: A generic fpga framework for graph neural network acceleration," *ArXiv*, vol. abs/2201.08475, 2022.

[2] A. Adinets, "A faster radix sort implementation," <https://www.nvidia.com/en-us/on-demand/session/gtcsj20-s21572/>, 2020.

[3] Alibaba, "User behavior data from taobao for recommendation," <https://tianchi.aliyun.com/dataset/649?lang=en-us>, 2018.

[4] AMD, "Vpk180 evaluation board user guide," <https://docs.amd.com/r/en-US/ug1582-vpk180-eval-bd>, 2023.

[5] AMD, "Amd kintex ultrascale fpga," 2025. [Online]. Available: <https://www.amd.com/ko/products/adaptive-soocs-and-fpgas/fpgas/kintex-ultrascale.html>

[6] AMD, "Xilinx sorting application user guide," 2025. [Online]. Available: <https://www.xilinx.com/content/dam/xilinx/publications/user-guide/db-sorting-user-guide.pdf>

[7] N. A. Asif, Y. Sarker, R. K. Chakrabortty, M. J. Ryan, M. H. Ahamed, D. K. Saha, F. R. Badal, S. K. Das, M. F. Ali, S. I. Moyeen, M. R. Islam, and Z. Tasneem, "Graph neural network: A comprehensive review on non-euclidean space," *IEEE Access*, 2021.

[8] M. Aumüller and N. Hass, "Simple and fast blockquicksort using lomuto's partitioning scheme," pp. 15–26, 2018.

[9] G. E. Blelloch, "Prefix sums and their applications," 1990.

[10] Z. Cai, X. Yan, Y. Wu, K. Ma, J. Cheng, and F. Yu, "Dgcl: An efficient communication library for distributed gnn training," in *Proceedings of the Sixteenth European Conference on Computer Systems*, 2021, pp. 130–144.

[11] A. Carter, A. Rodriguez, Y. Yang, and S. M. Meyer, "Nanosecond indexing of graph data with hash maps and vlists," *Proceedings of the 2019 International Conference on Management of Data*, 2019.

[12] C. Chen, K. Li, Y. Li, and X. Zou, "Regnn: A redundancy-eliminated graph neural networks accelerator," in *2022 IEEE International Symposium on High-Performance Computer Architecture (HPCA)*. IEEE, 2022, pp. 429–443.

[13] H.-C. Chen and C. Hao, "Dgnn-booster: A generic fpga accelerator framework for dynamic graph neural network inference," *2023 IEEE 31st Annual International Symposium on Field-Programmable Custom Computing Machines (FCCM)*, pp. 195–201, 2023.

[14] J. Chen, J. Zhu, and L. Song, "Stochastic training of graph convolutional networks with variance reduction," in *Proceedings of the 35th International Conference on Machine Learning, ICML 2018, Stockholmässan, Stockholm, Sweden, July 10-15, 2018*, ser. Proceedings of Machine Learning Research, J. G. Dy and A. Krause, Eds., vol. 80. PMLR, 2018, pp. 941–949. [Online]. Available: <http://proceedings.mlr.press/v80/chen18p.html>

[15] J. Chen, T. Ma, and C. Xiao, "Fastgcn: Fast learning with graph convolutional networks via importance sampling," *arXiv preprint arXiv:1801.10247*, 2018.

[16] R. Chen, S. Siriyal, and V. Prasanna, "Energy and memory efficient mapping of bitonic sorting on fpga," in *Proceedings of the 2015 ACM/SIGDA International Symposium on Field-Programmable Gate Arrays*, 2015, pp. 240–249.

[17] X. Chen, Y. Wang, X. Xie, X. Hu, A. Basak, L. Liang, M. Yan, L. Deng, Y. Ding, Z. Du, and Y. Xie, "Rubik: A hierarchical architecture for efficient graph neural network training," *IEEE Transactions on Computer-Aided Design of Integrated Circuits and Systems*, vol. 41, no. 4, pp. 936–949, 2021.

[18] Z. Chen, M. Yan, M. Zhu, L. Deng, G. Li, S. Li, and Y. Xie, "fuseggn: Accelerating graph convolutional neural network training on gpppu," in *Proceedings of the 39th International Conference on Computer-Aided Design*, 2020, pp. 1–9.

[19] E. Cohen, E. Halperin, H. Kaplan, and U. Zwick, "Reachability and distance queries via 2-hop labels," pp. 937–946, 2002.

[20] cornell, "Graphs and graph representations," <https://docs.amd.com/r/en-US/ug1582-vpk180-eval-bd>, 2020.

[21] K. Duan, Z. Liu, P. Wang, W. Zheng, K. Zhou, T. Chen, X. Hu, and Z. Wang, "A comprehensive study on large-scale graph training: Benchmarking and rethinking," *ArXiv*, vol. abs/2210.07494, 2022.

[22] C. Eksombatchai, P. Jindal, J. Z. Liu, Y. Liu, R. Sharma, C. Sugnet, M. Ulrich, and J. Leskovec, "Pixie: A system for recommending 3+ billion items to 200+ million users in real-time," in *Proceedings of the 2018 World Wide Web Conference on World Wide Web, WWW 2018, Lyon, France, April 23-27, 2018*, P. Champin, F. Gandon, M. Lalmas, and P. G. Ipeirotis, Eds. ACM, 2018, pp. 1775–1784. [Online]. Available: <https://doi.org/10.1145/3178876.3186183>

[23] W. Fan, Y. Ma, Q. Li, Y. He, E. Zhao, J. Tang, and D. Yin, "Graph neural networks for social recommendation," in *The World Wide Web Conference*, 2019, pp. 417–426.

[24] W. Fan, Y. Ma, Q. Li, J. Wang, G. Cai, J. Tang, and D. Yin, "A graph neural network framework for social recommendations," *IEEE Transactions on Knowledge and Data Engineering*, vol. 34, no. 5, pp. 2033–2047, 2020.

[25] M. Fey and J. E. Lenssen, "Fast graph representation learning with pytorch geometric," *arXiv preprint arXiv:1903.02428*, 2019.

[26] C. Gao, M. Afarin, S. Rahman, N. Abu-Ghazaleh, and R. Gupta, "Mega evolving graph accelerator," in *Proceedings of the 56th Annual IEEE/ACM International Symposium on Microarchitecture*, 2023, pp. 310–323.

[27] T. Geng, A. Li, R. Shi, C. Wu, T. Wang, Y. Li, P. Haghi, A. Turneo, S. Che, S. Reinhardt, and M. C. Herbordt, "Awb-gcn: A graph convolutional network accelerator with runtime workload rebalancing," in *2020 53rd Annual IEEE/ACM International Symposium on Microarchitecture (MICRO)*. IEEE, 2020, pp. 922–936.

[28] P. Gong, R. Liu, Z. Mao, Z. Cai, X. Yan, C. Li, M. Wang, and Z. Li, "gsampler: General and efficient gpu-based graph sampling for graph learning," in *Proceedings of the 29th Symposium on Operating Systems Principles*, 2023, pp. 562–578.

[29] Y. Gui, Q. Wu, W. Yuan, H. Liang, X. Wang, and X. Jin, "A fpga-hbm-based hardware streaming accelerator for gnn sampling," in *2024 IEEE 35th International Conference on Application-specific Systems, Architectures and Processors (ASAP)*. IEEE, 2024, pp. 77–78.

[30] Y. Gui, Q. Wu, W. Yuan, H. Liang, X. Wang, and X. Jin, "A fpga-hbm-based hardware streaming accelerator for GNN sampling," in *35th IEEE International Conference on Application-specific Systems, Architectures and Processors, ASAP 2024, Hong Kong, July 24-26, 2024*. IEEE, 2024, pp. 77–78. [Online]. Available: <https://doi.org/10.1109/ASAP61560.2024.00026>

[31] W. Hamilton, Z. Ying, and J. Leskovec, "Inductive representation learning on large graphs," in *Advances in Neural Information Processing Systems (NeurIPS)*, vol. 30, 2017.

[32] Y. Han, S. Karunasekera, and C. Leckie, "Graph neural networks with continual learning for fake news detection from social media," *arXiv preprint arXiv:2007.03316*, 2020.

[33] Y. Han, T. Kim, J. Kim, S. Ha, and L. Kim, "FLAG: an fpga-based system for low-latency GNN inference service using vector quantization," in *62nd ACM/IEEE Design Automation Conference, DAC 2025, San Francisco, CA, USA, June 22-25, 2025*. IEEE, 2025, pp. 1–7. [Online]. Available: <https://doi.org/10.1109/DAC63849.2025.11132631>

[34] M. Harris, "Parallel prefix sum (scan) with cuda," *GPU Gems*, vol. 3, 2007.

[35] X. He, K. Deng, X. Wang, Y. Li, Y. Zhang, and M. Wang, "Lightgcn: Simplifying and powering graph convolution network for recommendation," in *Proceedings of the International ACM SIGIR Conference on Research and Development in Information Retrieval (SIGIR)*, 2020.

[36] T. Hoefler, D. Alistarh, T. Ben-Nun, N. Dryden, and A. Peste, "Sparsity in deep learning: Pruning and growth for efficient inference and training in neural networks," *ArXiv*, vol. abs/2102.00554, 2021.

[37] Hu, Weihua, Fey, Matthias, Zitnik, Marinka, Dong, Yuxiao, Ren, Hongyu, Liu, Bowen, Catasta, Michele, Leskovec, and Jure, "Open graph benchmark: Datasets for machine learning on graphs," *arXiv preprint arXiv:2005.00687*, 2020.

[38] G. Huang, G. Dai, Y. Wang, and H. Yang, "Ge-spmm: General-purpose sparse matrix-matrix multiplication on gpus for graph neural networks," *SC20: International Conference for High Performance Computing, Networking, Storage and Analysis*, pp. 1–12, 2020.

[39] W. Huang, T. Zhang, Y. Rong, and J. Huang, "Adaptive sampling towards fast graph representation learning," in *Advances in Neural Information Processing Systems 31: Annual Conference on Neural Information Processing Systems 2018, NeurIPS 2018, December 3-8, 2018, Montréal, Canada*, S. Bengio, H. M. Wallach, H. Larochelle, K. Grauman, N. Cesa-Bianchi, and R. Garnett, Eds., 2018, pp. 4563–4572. [Online]. Available: <https://proceedings.neurips.cc/paper/2018/hash/01eee509ee2f68dc6014898c309e86bf-Abstract.html>

[40] K. Ji, B. Hui, and G. Luo, "Graph attention networks with local structure awareness for knowledge graph completion," *IEEE Access*, vol. 8, pp. 224 860–224 870, 2020.

[41] D. Juenger, N. Iskos, Y. Wang, J. Hemstad, C. Hundt, and N. Sakharnykh, “Maximizing performance with massively parallel hash maps on gpus,” <https://developer.nvidia.com/blog/maximizing-performance-with-massively-parallel-hash-maps-on-gpus/>, 2023.

[42] T. Kaler, N. Stathas, A. Ouyang, A. Iliopoulos, T. Schardl, C. Leiserson, and J. Chen, “Accelerating training and inference of graph neural networks with fast sampling and pipelining,” *ArXiv*, vol. abs/2110.08450, 2021.

[43] T. Kaler, N. Stathas, A. Ouyang, A. Iliopoulos, T. B. Schardl, C. E. Leiserson, and J. Chen, “Accelerating training and inference of graph neural networks with fast sampling and pipelining,” in *Proceedings of the Fifth Conference on Machine Learning and Systems, MLSys 2022, Santa Clara, CA, USA, August 29 - September 1, 2022*, D. Marculescu, Y. Chi, and C. Wu, Eds. mlsys.org, 2022. [Online]. Available: https://proceedings.mlsys.org/paper_files/paper/2022/hash/afacc5db3e0e85b446e6c7727cd7dca5-Abstract.html

[44] K. Kiningham, P. Levis, and C. Ré, “Grip: A graph neural network accelerator architecture,” *IEEE Transactions on Computers*, vol. 72, no. 4, pp. 914–925, 2022.

[45] T. N. Kipf and M. Welling, “Semi-supervised classification with graph convolutional networks,” 2017.

[46] K. Kiwi, “Partitioning schemes for quicksort and quickselect,” *ArXiv*, vol. cs.DS/0312054, 2003.

[47] D. Koch and J. Tørresen, “Fpgasort: a high performance sorting architecture exploiting run-time reconfiguration on fpgas for large problem sorting,” in *Symposium on Field Programmable Gate Arrays*, 2011.

[48] V. Lai and O. Diessel, “Icap-i: A reusable interface for the internal reconfiguration of xilinx fpgas,” in *International Conference on Field-Programmable Technology*, 2009, pp. 357–360.

[49] C. lee Chang and R. Melhem, “Arbitrary size benes networks,” *Parallel Process. Lett.*, vol. 7, pp. 279–284, 1997.

[50] W. Lei, G. Zhang, X. He, Y. Miao, X. Wang, L. Chen, and T.-S. Chua, “Interactive path reasoning on graph for conversational recommendation,” in *Proceedings of the ACM SIGKDD International Conference on Knowledge Discovery & Data Mining (SIGKDD)*, 2020.

[51] J. Leskovec and A. Krevl, “SNAP Datasets: Stanford large network dataset collection,” <http://snap.stanford.edu/data>, Jun. 2014.

[52] S. Li, D. Niu, Y. Wang, W. Han, Z. Zhang, T. Guan, Y. Guan, H. Liu, L. Huang, Z. Du, F. Xue, Y. Fang, H. Zheng, and Y. Xie, “Hyperscale fpga-as-a-service architecture for large-scale distributed graph neural network,” in *Proceedings of the 49th Annual International Symposium on Computer Architecture*, 2022, pp. 946–961.

[53] S. Li, D. Niu, Y. Wang, W. Han, Z. Zhang, T. Guan, Y. Guan, H. Liu, L. Huang, Z. Du, F. Xue, Y. Fang, H. Zheng, and Y. Xie, “Hyperscale fpga-as-a-service architecture for large-scale distributed graph neural network,” in *ISCA '22: The 49th Annual International Symposium on Computer Architecture, New York, New York, USA, June 18 - 22, 2022*, V. Salapura, M. Zahran, F. Chong, and L. Tang, Eds. ACM, 2022, pp. 946–961. [Online]. Available: <https://doi.org/10.1145/3470496.3527439>

[54] Y. Li, T.-Y. Yang, M.-C. Yang, Z. Shen, and B. Li, “Celeritas: Out-of-core based unsupervised graph neural network via cross-layer computing 2024,” *2024 IEEE International Symposium on High-Performance Computer Architecture (HPCA)*, pp. 91–107, 2024.

[55] S. Liang, C. Liu, Y. Wang, H. Li, and X. Li, “Deepburning-gl: an automated framework for generating graph neural network accelerators,” in *Proceedings of the 39th International Conference on Computer-Aided Design*, 2020, pp. 1–9.

[56] S. Liang, Y. Wang, C. Liu, L. He, L. Huawei, D. Xu, and X. Li, “Engn: A high-throughput and energy-efficient accelerator for large graph neural networks,” *IEEE Transactions on Computers*, vol. 70, no. 9, pp. 1511–1525, 2020.

[57] D. Lin, S. Sun, J. Ding, X. Ke, H. Gu, X. Huang, C. Song, X. Zhang, L. Yi, J. Wen, and C. Chen, “Platogl: Effective and scalable deep graph learning system for graph-enhanced real-time recommendation,” in *Proceedings of the 31st ACM International Conference on Information & Knowledge Management, Atlanta, GA, USA, October 17-21, 2022*, M. A. Hasan and L. Xiong, Eds. ACM, 2022, pp. 3302–3311. [Online]. Available: <https://doi.org/10.1145/3511808.3557084>

[58] X. Liu, M. Yan, L. Deng, G. Li, X. Ye, and D. Fan, “Sampling methods for efficient training of graph convolutional networks: A survey,” *IEEE/CAA Journal of Automatica Sinica*, vol. 9, pp. 205–234, 2021.

[59] X. Liu, M. Yan, S. Song, Z. Lv, W. Li, G. Sun, X. Ye, and D. Fan, “Gnnampler: Bridging the gap between sampling algorithms of gnn and hardware,” pp. 498–514, 2021.

[60] X. Liu, S. Li, K. Fang, Y. Ni, Z. Li, and Y. Deng, “Radixboost: A hardware acceleration structure for scalable radix sort on graphic processors,” in *2015 IEEE International Symposium on Circuits and Systems (ISCAS)*. IEEE, 2015, pp. 1174–1177.

[61] L. Ma, Z. Yang, Y. Miao, J. Xue, M. Wu, L. Zhou, and Y. Dai, “{NeuGraph}: Parallel deep neural network computation on large graphs,” in *2019 USENIX Annual Technical Conference (USENIX ATC 19)*, 2019, pp. 443–458.

[62] D. S. Miller, R. Henderson, and J. Jelinek, “Dynamic dma mapping guide,” <https://www.kernel.org/doc/html/v6.12/core-api/dma-api-howto.html>.

[63] H. Mostafa, A. Grabowski, M. A. Turja, J. Cerviño, A. Ribeiro, and N. Himayat, “Fastsample: Accelerating distributed graph neural network training for billion-scale graphs,” *ArXiv*, vol. abs/2311.17847, 2023.

[64] D. Nathani, J. Chauhan, C. Sharma, and M. Kaul, “Learning attention-based embeddings for relation prediction in knowledge graphs,” *arXiv preprint arXiv:1906.01195*, 2019.

[65] NVIDIA, “Nvidia ampere ga102 gpu architecture,” <https://www.nvidia.com/content/PDF/nvidia-ampere-ga-102-gpu-architecture-whitepaper-v2.1.pdf>.

[66] L. Pezzarossa, M. Schoeberl, and J. Sparsø, “A controller for dynamic partial reconfiguration in fpga-based real-time systems,” *2017 IEEE 20th International Symposium on Real-Time Distributed Computing (ISORC)*, pp. 92–100, 2017.

[67] Y. Saad, “Iterative methods for sparse linear systems,” 2003, pp. I–XVIII, 1–528.

[68] M. Saitoh and K. Kise, “Very massive hardware merge sorter,” in *2018 International Conference on Field-Programmable Technology (FPT)*. IEEE, 2018, pp. 86–93.

[69] R. Sarkar, S. Abi-Karam, Y. He, L. Sathidevi, and C. Hao, “Flowgnn: A dataflow architecture for real-time workload-agnostic graph neural network inference,” in *2023 IEEE International Symposium on High-Performance Computer Architecture (HPCA)*. IEEE, 2023, pp. 1099–1112.

[70] W. Shi and R. Rajkumar, “Point-gnn: Graph neural network for 3d object detection in a point cloud,” in *Proceedings of the IEEE/CVF conference on computer vision and pattern recognition*, 2020, pp. 1711–1719.

[71] Shlomi, Jonathan, Battaglia, Peter, Vlimant, and Jean-Roch, “Graph neural networks in particle physics,” *Machine Learning: Science and Technology*, vol. 2, no. 2, p. 021001, 2020.

[72] W. Song, D. Koch, M. Luján, and J. Garside, “Parallel hardware merge sorter,” *2016 IEEE 24th Annual International Symposium on Field-Programmable Custom Computing Machines (FCCM)*, pp. 95–102, 2016.

[73] J. Sun, Z. Shi, L. Su, W. Shen, Z. Wang, Y. Li, W. Yu, W. Lin, F. Wu, B. He, and J. Zhou, “Helios: Efficient distributed dynamic graph sampling for online GNN inference,” in *Proceedings of the 30th ACM SIGPLAN Annual Symposium on Principles and Practice of Parallel Programming, PPoPP 2025, Las Vegas, NV, USA, March 1-5, 2025*. ACM, 2025, pp. 2–15. [Online]. Available: <https://doi.org/10.1145/3710848.3710854>

[74] Q. Sun, Y. Liu, H. Yang, R. Zhang, M. Dun, M. Li, X. Liu, W. Xiao, Y. Li, Z. Luan *et al.*, “Cognn: efficient scheduling for concurrent gnn training on gpus,” in *SC22: International Conference for High Performance Computing, Networking, Storage and Analysis*. IEEE, 2022, pp. 1–15.

[75] A. Tripathy, K. Yelick, and A. Buluç, “Reducing communication in graph neural network training,” *SC20: International Conference for High Performance Computing, Networking, Storage and Analysis*, pp. 1–20, 2020.

[76] J. Vatter, R. Mayer, and H. Jacobsen, “The evolution of distributed systems for graph neural networks and their origin in graph processing and deep learning: A survey,” *ACM Computing Surveys*, vol. 56, pp. 1 – 37, 2023.

[77] P. Veličković, G. Cucurull, A. Casanova, A. Romero, P. Lio, and Y. Bengio, “Graph attention networks,” *arXiv preprint arXiv:1710.10903*, 2017.

[78] J. S. Vitter, “Random sampling with a reservoir,” *ACM Transactions on Mathematical Software (TOMS)*, vol. 11, no. 1, pp. 37–57, 1985.

[79] M. Wang, D. Zheng, Z. Ye, Q. Gan, M. Li, X. Song, J. Zhou, C. Ma, L. Yu, Y. Gai, T. Xiao, T. He, G. Karypis, J. Li, and Z. Zhang, “Deep graph library: A graph-centric, highly-performant package for graph neural networks,” *arXiv preprint arXiv:1909.01315*, 2019.

[80] X. Wang and M. Zhang, “How powerful are spectral graph neural networks,” in *International Conference on Machine Learning, ICML 2022, 17-23 July 2022, Baltimore, Maryland, USA*, ser. Proceedings of Machine Learning Research, K. Chaudhuri, S. Jegelka, L. Song, C. Szepesvári, G. Niu, and S. Sabato, Eds., vol. 162. PMLR, 2022, pp. 23341–23362. [Online]. Available: <https://proceedings.mlr.press/v162/wang22am.html>

[81] Y. Wang, B. Feng, G. Li, S. Li, L. Deng, Y. Xie, and Y. Ding, “{GNNAdvisor}: An adaptive and efficient runtime system for {GNN} acceleration on {GPUs},” in *15th USENIX symposium on operating systems design and implementation (OSDI 21)*, 2021, pp. 515–531.

[82] M. Wilcox and A. Cox, “Bus-independent device accesses,” <https://www.kernel.org/doc/html/latest/driver-api/device-io.html>.

[83] S. Wu, F. Sun, W. Zhang, and B. Cui, “Graph neural networks in recommender systems: a survey,” *arXiv preprint arXiv:2011.02260*, 2020.

[84] Z. Wu, S. Pan, F. Chen, G. Long, C. Zhang, and S. Y. Philip, “A comprehensive survey on graph neural networks,” *IEEE transactions on neural networks and learning systems*, vol. 32, no. 1, pp. 4–24, 2020.

[85] G. Xiao, L. Xia, Y. Chen, H. Chen, and W. Yang, “Dcgg: A dynamically adaptive and hardware-software coordinated runtime system for gnn acceleration on gpus,” *IEEE Transactions on Computers*, 2025.

[86] Xilinx, “Logicore ip axi hwicap product specification,” https://docs.amd.com/v/u/en-US/ds817_axi_hwicap.

[87] M. Yan, L. Deng, X. Hu, L. Liang, Y. Feng, X. Ye, Z. Zhang, D. Fan, and Y. Xie, “Hygen: A gcn accelerator with hybrid architecture,” in *IEEE International Symposium on High Performance Computer Architecture (HPCA)*. IEEE, 2020, pp. 15–29.

[88] R. Ying, R. He, K. Chen, P. Eksombatchai, W. L. Hamilton, and J. Leskovec, “Graph convolutional neural networks for web-scale recommender systems,” in *Proceedings of the ACM SIGKDD International Conference on Knowledge Discovery & Data Mining (SIGKDD)*, 2018.

[89] H. You, T. Geng, Y. Zhang, A. Li, and Y. Lin, “Geod: Graph convolutional network acceleration via dedicated algorithm and accelerator co-design,” *2022 IEEE International Symposium on High-Performance Computer Architecture (HPCA)*, pp. 460–474, 2021.

[90] D. Yu, Y. Yang, R. Zhang, and Y. Wu, “Knowledge embedding based graph convolutional network,” in *Proceedings of the Web Conference, 2021*, pp. 1619–1628.

[91] H. Yuan, J. Tang, X. Hu, and S. Ji, “Xgnn: Towards model-level explanations of graph neural networks,” in *Proceedings of the 26th ACM SIGKDD international conference on knowledge discovery & data mining*, 2020, pp. 430–438.

[92] H. Zeng and V. Prasanna, “Graphact: Accelerating gcn training on cpu-fpga heterogeneous platforms,” in *proceedings of the 2020 ACM/SIGDA international symposium on field-programmable gate arrays*, 2020, pp. 255–265.

[93] H. Zeng, H. Zhou, A. Srivastava, R. Kannan, and V. Prasanna, “Graphsaint: Graph sampling based inductive learning method,” *arXiv preprint arXiv:1907.04931*, 2019.

[94] B. Zhang, R. Kannan, and V. Prasanna, “Boostgcn: A framework for optimizing gcn inference on fpga,” in *2021 IEEE 29th Annual International Symposium on Field-Programmable Custom Computing Machines (FCCM)*. IEEE, 2021, pp. 29–39.

[95] B. Zhang, H. Zeng, and V. Prasanna, “Hardware acceleration of large scale gcn inference,” in *2020 IEEE 31st International Conference on Application-specific Systems, Architectures and Processors (ASAP)*. IEEE, 2020, pp. 61–68.

[96] D. Zhang, X. Huang, Z. Liu, J. Zhou, Z. Hu, X. Song, Z. Ge, L. Wang, Z. Zhang, and Y. Qi, “Agl: a scalable system for industrial-purpose graph machine learning,” *arXiv preprint arXiv:2003.02454*, 2020.

[97] G. Zhang, N. Attaluri, J. Emer, and D. Sánchez, “Gamma: leveraging gustavson’s algorithm to accelerate sparse matrix multiplication,” *Proceedings of the 26th ACM International Conference on Architectural Support for Programming Languages and Operating Systems*, 2021.

[98] Z. Zhang, F. Zhuang, H. Zhu, Z. Shi, H. Xiong, and Q. He, “Relational graph neural network with hierarchical attention for knowledge graph completion,” in *Proceedings of the AAAI Conference on Artificial Intelligence (AAAI)*, vol. 34, 2020, pp. 9612–9619.

[99] J. Zhao, Z. Zhou, Z. Guan, W. Zhao, W. Ning, G. Qiu, and X. He, “Intentgc: A scalable graph convolution framework fusing heterogeneous information for recommendation,” in *Proceedings of the 25th ACM SIGKDD International Conference on Knowledge Discovery & Data Mining, KDD 2019, Anchorage, AK, USA, August 4-8, 2019*, A. Teredesai, V. Kumar, Y. Li, R. Rosales, E. Terzi, and G. Karypis, Eds. ACM, 2019, pp. 2347–2357. [Online]. Available: <https://doi.org/10.1145/3292500.3330686>

[100] D. Zheng, X. Song, C. Yang, D. LaSalle, and G. Karypis, “Distributed hybrid cpu and gpu training for graph neural networks on billion-scale heterogeneous graphs,” in *Proceedings of the 28th ACM SIGKDD Conference on Knowledge Discovery and Data Mining*, 2022, pp. 4582–4591.

[101] J. Zhou, G. Cui, S. Hu, Z. Zhang, C. Yang, Z. Liu, L. Wang, C. Li, and M. Sun, “Graph neural networks: A review of methods and applications,” *AI open*, vol. 1, pp. 57–81, 2020.

[102] D. Zou, Z. Hu, Y. Wang, S. Jiang, Y. Sun, and Q. Gu, “Layer-dependent importance sampling for training deep and large graph convolutional networks,” in *Advances in Neural Information Processing Systems 32: Annual Conference on Neural Information Processing Systems 2019, NeurIPS 2019, December 8-14, 2019, Vancouver, BC, Canada*, H. M. Wallach, H. Larochelle, A. Beygelzimer, F. d’Alché-Buc, E. B. Fox, and R. Garnett, Eds., 2019, pp. 11247–11256. [Online]. Available: <https://proceedings.neurips.cc/paper/2019/hash/91ba4a4478a66bee9812b0804b6f9d1b-Abstract.html>